Vietnam Journal of Earth Sciences, 41(4), 305–320, Doi: 10.15625/0866-7187/41/4/14234

(VAST)

Vietnam Academy of Science and Technology

Vietnam Journal of Earth Sciences

http://www.vjs.ac.vn/index.php/jse

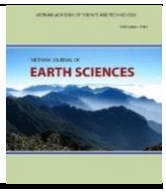


# Ground displacement of the 6 July 2019 Ridgecrest earthquake from the GNSS permanent stations

Nguyen Ngoc Lau[1], Phan Trong Trinh[2, 3, 4*], Tran Van Phong[2], Binh Thai Pham[5]

[1]*Ho Chi Minh City University of Technology, Vietnam*
[2]*Institute of Geological Sciences, VAST, Hanoi, Vietnam*
[3]*Royal Academy for Oversea Sciences, Brussels, Belgium*
[4]*Graduate University of Science and Technology, VAST, Hanoi, Vietnam*
[5]*University of Transport Technology, Hanoi 100000, Vietnam*

Received 14 July 2019; Received in revised form 20 August 2019; Accepted 1 September 2019

ABSTRACT

The Eastern California earthquake (also known as the Ridgecrest earthquake) occurred at 03:19:53 (UTC) on the 6th of July, with a moment magnitude of 7.1. Over the region, there is an accurate network of GNSS permanent stations. Precise determination of displacements of these stations will provide important information to better understand the structure and scope of the earthquake, contributing to faster and more accurate earthquake prediction. In this paper, we used precise point positioning with ambiguity resolution to determine the co-seismic displacements of 25 GNSS stations around the epicenter for the day of the earthquake. The processing results show that the affected area being more than 100 km centered around the earthquake epicenter with the largest value being approximately 0.6 m.

*Keywords:* Co-seismic ground díplacement; 2019 Ridgecrest earthquake; GNSS; PPP; California.



## 1. Introduction

The July 6th, 2019, 03:19:53 UTC Mw 7.1 earthquake in eastern California, southwest of Searles Valley, occurred as the result of shallow strike-slip faulting in the crust of the North America plate. Focal mechanism solutions for the earthquake indicate rupture occurred on a steeply dipping fault as the result of either right-lateral slip on a plane striking NW-SE, or as left-lateral slip on a plane striking SW-NE (USGS, 2019). At the location of this earthquake, approximately 150 km northeast of San Andreas Fault-the major plate boundary in the region-the Pacific plate moves to the northwest with respect to the North America plate at a rate of approximately 48 mm/yr. The location of the earthquake falls within the Eastern California shear zone, a region of distributed faulting associated with motion across the Pacific: North America plate boundary, and an area of high seismic hazard.

According to the United States Geological Survey (USGS, 2019), this earthquake occurred approximately 34 hours after and 11 km northwest of an M 6.4 event in the same region, on July 4th, 2019, at 17:33 UTC.

*Corresponding author, Email: phantrongt.igs@gmail.com

The July 4th event was preceded by a short series of small foreshocks (including an M4.0 earthquake 30 minutes prior) and was followed by a robust sequence of aftershocks, including almost 250 M 2.5+ earthquakes (up until the M 7.1 event). Those events aligned with both nodal planes (NE-SW and NW-SE) of the focal mechanism solution of the M 6.4 event, which was very similar in faulting style to today's M 7.1 earthquake. The sequence includes two other M5+ earthquakes, one of which occurred 20 seconds before the M 7.1 event. The M 7.1 earthquake occurred at the NW extension of the prior sequence.

This region of eastern California has hosted numerous moderate-sized earthquakes. Over the past 40 years, prior to the July 4th event, 8 other M5+ earthquakes have occurred within 50 km of the July 6th, 2019 earthquake. The largest of these was an M 5.8 event on September 20, 1995, just 3 km to the west of today's event, which was felt strongly in the China Lake-Ridgecrest area, and more broadly from Los Angeles to Las Vegas. Cover this region is an accurate state-of-the-art network of GNSS control stations, which is established and maintained by the California Spatial Reference Center (CSRC). The CSRC was established in 1997 as a partnership with surveyors, engineers, GIS professionals, the National Geodetic Survey (NGS), the California Department of Transportation (Caltrans), and the geodetic and geophysical communities.

The CSRC is operated by the Scripps Orbit and Permanent Array Center (SOPAC, 2019) located at the Cecil H. and Ida M. Green Institute of Geophysics and Planetary Physics (IGPP) at Scripps Institution of Oceanography. The data of the GNSS network can be accessed freely through the SOPAC Data Archive as they become available.

This paper aims to determine more precision of co-seismic ground displacement of the 6 July 2019 Ridgecrest earthquake from GNSS Precise Point Positioning (PPP) and compare to the Real-time determination of SOPAC. With SOPAC support, we collected some GNSS data from 25 GNSS stations around the epicenter on the day of the earthquake. These stations are listed in Table 1. This high-rate permanent GNSS station network with a density of 15-20km/point is a favorable condition for applying existing GNSS positioning methods to accurately determine the displacement of the station over time.

*Table 1*. GNSS stations are located around the epicenter

| No. | GNSS Station | Interval (sec) | GNNS satellite systems | Distance to the epicenter (km) |
|---|---|---|---|---|
| 1 | P595 | 15 | GPS | 19.5 |
| 2 | P594 | 15 | GPS | 23.7 |
| 3 | CCCC | 15 | GPS | 23.9 |
| 4 | COSO | 30 | GPS | 30.0 |
| 5 | P580 | 15 | GPS | 40.5 |
| 6 | BEPK | 15 | GPS | 44.5 |
| 7 | P464 | 15 | GPS, GLONASS, GALILEO | 46.0 |
| 8 | P616 | 15 | GPS, GLONASS, GALILEO | 46.7 |
| 9 | P463 | 15 | GPS | 48.4 |
| 10 | RAMT | 15 | GPS | 48.6 |
| 11 | P593 | 15 | GPS | 55.5 |
| 12 | P570 | 15 | GPS | 60.9 |
| 13 | P597 | 15 | GPS | 64.4 |
| 14 | P569 | 15 | GPS | 64.5 |
| 15 | P592 | 15 | GPS | 64.9 |
| 16 | P573 | 15 | GPS | 69.4 |
| 17 | GOL2 | 30 | GPS | 74.8 |
| 18 | P590 | 15 | GPS, GLONASS, GALILEO | 75.8 |
| 19 | CPBN | 15 | GPS | 77.6 |
| 20 | P591 | 15 | GPS, GLONASS | 78.3 |
| 21 | P466 | 15 | GPS, GLONASS, GALILEO | 86.2 |
| 22 | P465 | 15 | GPS | 90.9 |
| 23 | LNMT | 15 | GPS | 96.3 |
| 24 | P615 | 15 | GPS | 98.4 |
| 25 | P617 | 15 | GPS | 105.9 |

## 2. Tectonic setting

The earthquake with M = 7.1 destroyed at least 35 km from the epicenter on July 6, 2019, about northwest, and 25 km southeast. However, there was no continuous observation on the ground, although no

vegetation could hide the faults. Many other faults have been mapped in this area, mainly north-south. However, the aftershock distribution extends in the northwest-southeast direction, indicating a continuous fault. The strike is parallel to the San Andreas Fault, but there is a more western direction than most of the surrounding faults. Unknowing of this fault, one has no reason to suspect that such a large earthquake could occur in the north of rupture on July 6. While most aftershocks in the past 48 hours have been distributed along two nearly linear faults, the aftershock of this 7.1-magnitude earthquake formed a cluster in the northwest of the main fault. This cluster, near Little Lake, CA, is about 15 km south of Geothermal Area Coso. The geothermal region that is home to a rich seismic is often concentrated in the herd in the periphery. All events in this group, are shallower than 10 km deep, suitable for previous groups in this area (Stein et al., 2019a; 2019b).

The general context of the Ridgecrest earthquake is the Eastern California shear zone (ECSZ) located to the east of the southern section of the San Andreas fault (SAF) and coinciding with the Mojave desert. It is cut by the Garlock fault, extending northeast and east from SAF to the Death Valley fault near the Nevada state boundary, passing Ridgecrest about 25 km to the South. ECSZ is associated with Walker Lane, a fault zone that runs east of the Sierra Nevada and into Nevada. That's where the Sierra Nevada block is the basis for most Central California being pulled out of North America. About a quarter of the slippage between the Pacific and North American segments is provided through ECSZ and Walker Lane. To the north of the Garlock Fault, the western edge of ECSZ is the Sierra Nevada fault running near California Highway 14 west of Ridgecrest. They then went into Coso Volcanic School, a complex fault zone, where the stress and slipping movement from Owens Valley's fault to the north was transferred to various faults, including the Panamint Valley fault at East. The 2019 earthquake occurred in which the striking Little fracture on the right crossed the Lake Complex fault zone extending north. This area is covered by a thick layer of silt; The surface expression of the fracture is a series of small normal faults (Fig. 1).

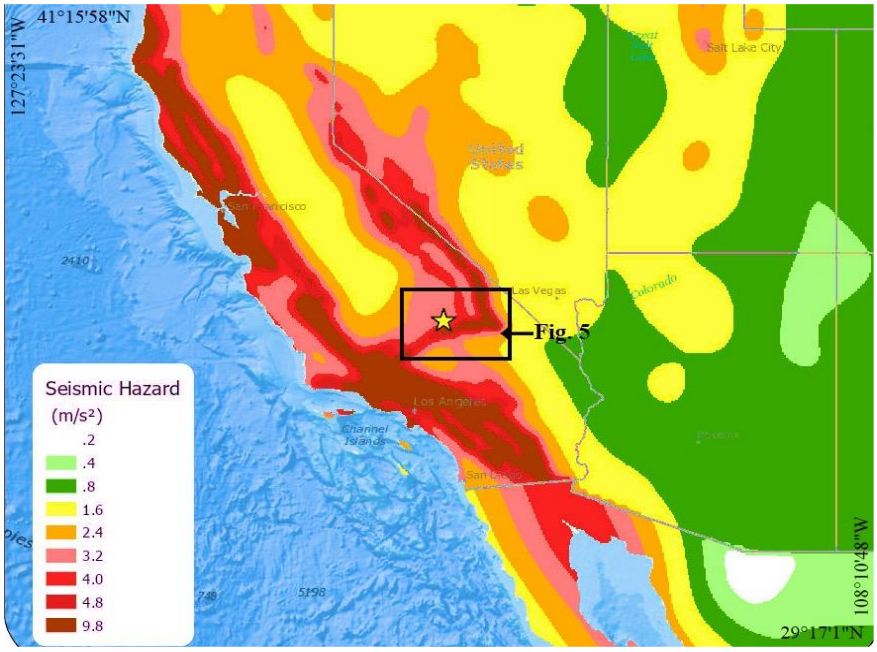


*Figure 1*. Epicenter of the M7.1 Ridgecrest earthquake and main seismic zones in California (modified from USGS)

## 3. Data and Method

### *3.1. Data*

The CSRC is operated by the Scripps Orbit and Permanent Array Center (SOPAC) located at the Cecil H. and Ida M. Green Institute of Geophysics and Planetary Physics (IGPP) at Scripps Institution of Oceanography. The data of the GNSS network can be accessed freely through the SOPAC Data Archive as they become available (SOPAC, 2019).

Data on recent earthquakes have also been collected and processed using GNSS (Ji C. et al., 2004; Yue H. et al., 2013, Kouba, 2009). By GNSS technology, we can accurately determine the displacement of each GNSS station. Previous studies often use relative positioning methods. Recently scientists focus to exploit more advanced precise point positioning methods (PPP). PPP with ambiguity resolution (AR) is also the method we choose to use for this paper. It will, therefore, be introduced in more detail in Section 2.

The Advanced Rapid Imaging and Analysis (ARIA) team used synthetic aperture radar (SAR) images Sentinel-1 from before and after the series of earthquakes- July 4 and July 10, 2019, respectively to create the map showing areas that are damaged as a result of the major earthquakes in Southern California. The color variation from yellow to red indicates an increasingly more significant surface change or damage. The map covers an area of 250 by 300 kilometers. Each pixel measures about 30 meters across. The map may be less reliable over vegetated areas but can provide useful guidance in identifying damaged areas. These datasets are helping local authorities assess the damage and will also provide useful information for us to map active fault. Synthetic aperture radar (SAR) images are also provided by the Geospatial Information Authority of Japan.

### *3.2. GNSS Precise Positioning Point with ambiguity resolution*

PPP was studied starting in 1997 (Zumberge J.F. et al., 1997). PPP differs from the usual absolute positioning methods in that it deals with GNSS carrier phase measurements and uses precise products of coordinates and clock corrections of GNSS satellites. Therefore the positioning accuracy of PPP can be achieved at the cm level when dealing with static 24 hours data and dm when kinematic processing (Zumberge J.F. et al., 1997; King M. et al., 2002).

In relative positioning, data of at least two receivers are processed simultaneously to provide baseline vectors. The accuracy of the method depends on the distance between the receivers. Meanwhile PPP only uses a single receiver so it is not affected by this factor (King M. et al., 2002).

The positioning accuracy of PPP can be improved by processing integrated multiple satellite systems (mutlti-GNSS PPP) and multivalued treatment for phase measurement (PPP-AR). (Rabbou M.A. et al., 2015; Afifi A. et al., 2016) have shown that PPP with multi-GNSS potentially can provide an accuracy of better than 1cm in 24h static and better than 1 decimeter in kinematic modes. Another important direction focuses on resolving ambiguity for carrier phase measurements (Geng J. et al., 2012; Laurichesse, 2012).

According to Seepersad and Bisnath (2016), there are currently three approaches to creating PPP ambiguity resolution (PPP-AR) products: FCB (Fractional Cycle Bias - Partial Cycle), IRC (Integer Recovery Clock - Resurrection Clock) (Laurichesse, 2012) and DC (Decoupled Clock) (Shi, 2012). For PPP users, the mathematical model of the above three methods is similar. These PPP-AR products are different but contain the same information. Therefore they can be converted from one form to another. An overview of the different suppliers and their products is shown in Fig. 2.

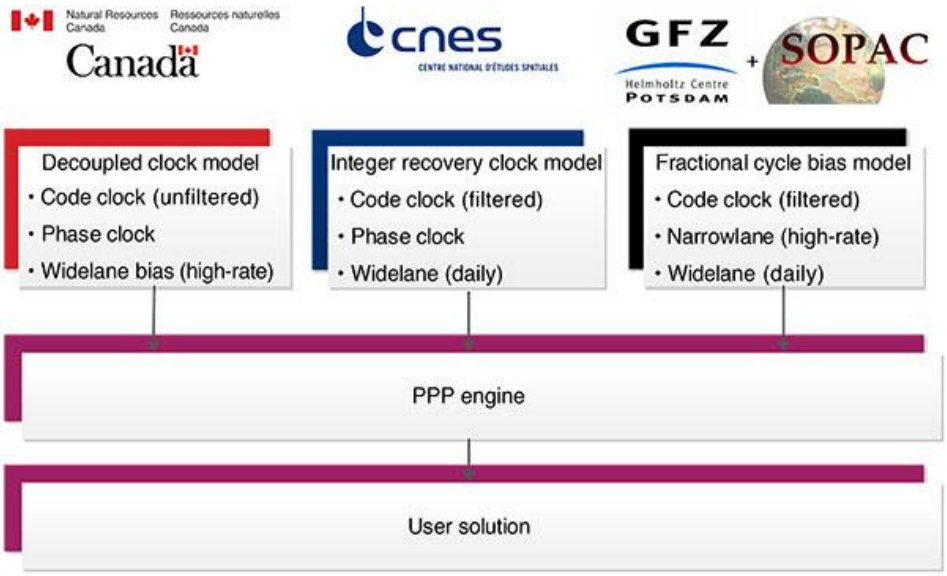


*Figure 2*. Some suppliers of PPP-AR products referred from (Seepersad and Bisnath, 2016)

It should be emphasized that all PPP-AR products currently only serve for GPS. Therefore, solving ambiguity parameters in PPP is currently only possible for GPS measurements.

Chen and Wang (2016) compared the PPP results when using PPP-AR products in the form of IRC and FCB and concluded that although these methods are identical in theory, in fact, IRC based on PPP-AR works a little better than the FCB based on the PPP-AR due to the systematic error of FCB estimation.

In Vietnam, we have studied PPP since 2010. The result of this study is our self-developed software called PPPC. Initially, the software was only capable of handling GPS measurements, then expanded to GPS and GLONASS (Nguyen L.N. et al., 2012). PPPC was first used for the purpose of studying ground movement due to the Gorkha earthquake in Nepal on the 25th of April, 2015. Recently, we have upgraded the software to add ambiguity resolution capabilities for GPS only when using CNES (Centre National d'Etudes Spatiales) products. CNES is currently one of the 12 analysis centers that contribute to the product of the GPS, GLONASS and GALILEO orbit and clock corrections for the IGS. More specifically, its products support for resolving ambiguity of PPP (Laurichesse, 2012). (Nguyen L.N., 2017) showed that the accuracies of PPP with AR for 24h static data are 1.9, 2.8 and 5.5 mm for the East, North and Up components respectively. These accuracies are improved mostly on the East (30%) and Up (10%) components compared with the case without using AR (2.7, 3.0, 6.1) mm. The epoch solutions with AR can provide accuracies of (8, 9, 28) mm, which are better than those without AR (13, 13, 38) mm.

With the accuracy achieved by PPP-AR, the application of it to the monitoring of ground movement in a slow or abrupt state will allow the determination of a more precise shift than the traditional PPP method. In this article, we use PPPC with AR to process GNSS data in Table 1.

## 4. Processing results

The GNSS data of all stations in Table 1 are processed by PPPC software in kinematic mode, with the following settings:

- Using CNES precise orbit and clock corrections
- Using P3 code and L3 carrier phase measurements of GPS only with ambiguity resolution
- Setting the elevation cut off angle as 5°
- Estimating one tropospheric zenith delay every 2.5 hours with the Niell mapping function
- Applying IGS14 antenna model and solid Earth model

After screening the processed station coordinates epoch by epoch, we detect the 8 closest stations which have the largest slip values at epoch 3:20:15 (GPST) as shown in Fig. 3. Therefore at the time of the earthquake (3:19:53 UTC ~ 3:20:11 GPST), the stations were mostly affected immediately.

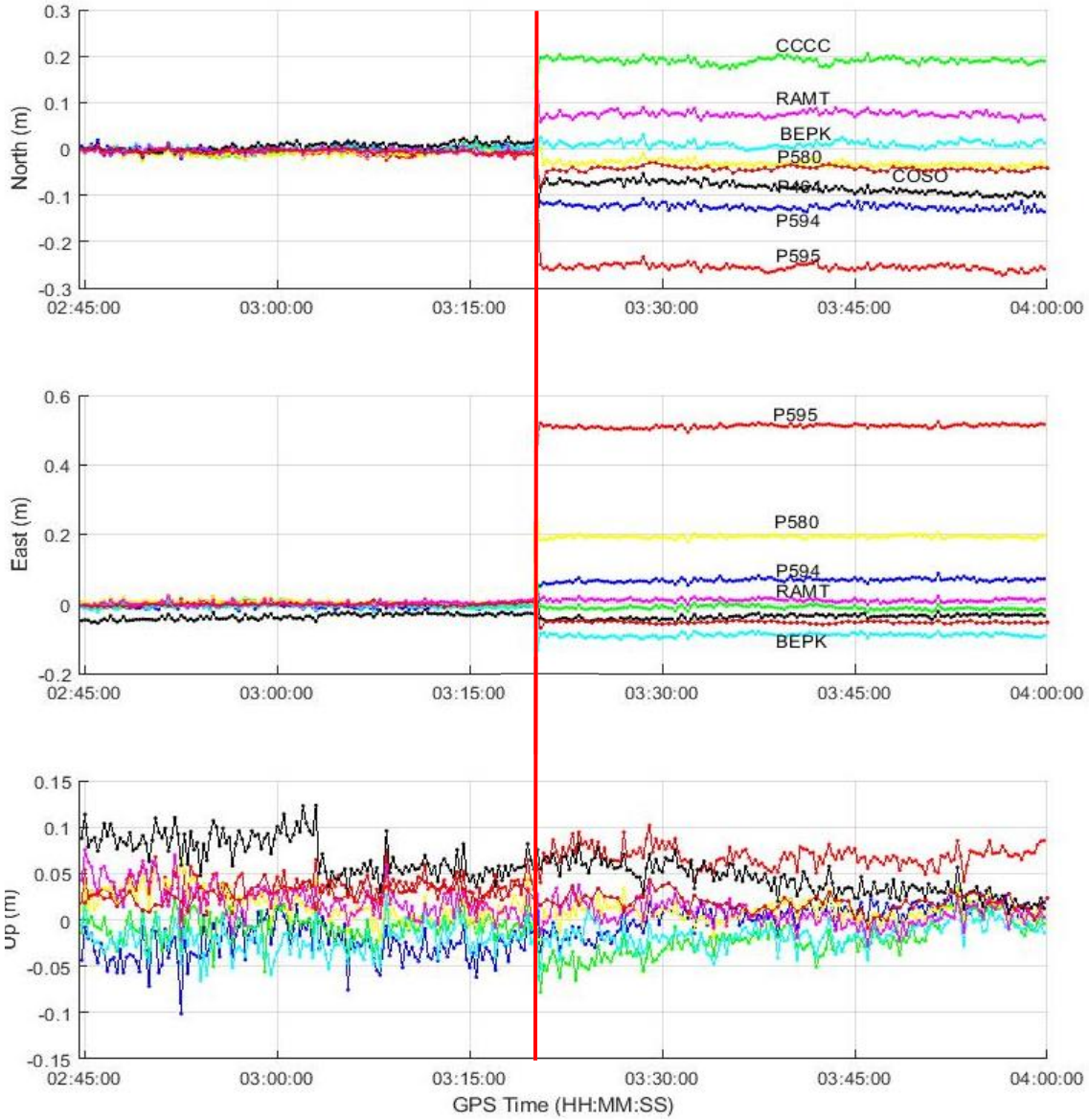


*Figure 3*. Station displacements by using PPPC in kinematic mode. Vertical bar indicates the earthquake epoch

GNSS epoch solutions with AR have accuracy at the centimeter level. To obtain more accuracy, we re-processed the GNSS data by using PPPC in static mode for epochs before and after epoch 3:20:15. For the station coordinates before the earthquake, we process data of the whole 5th of July and apart of 6th of July to epoch 3:20:15. The data after epoch 3:20:15 are chosen from this epoch to the rest of the day. As a result, the displacement of each station is calculated by subtracting two processed station coordinates before and after epoch 3:20:15. These results are given in Table 2.

*Table 2*. Coordinates in ITRF2014 before and displacements of GNSS stations after epoch 3:20:15 GPST

| No. | GNSS Station | Coordinates in ITRF2014 (m) | | | Displacements (m) | | |
|---|---|---|---|---|---|---|---|
| | | X | Y | Z | North | East | Up |
| 1 | P595 | -2386904.625 | -4604247.845 | 3701367.061 | -0.251 ±0.001 | +0.516 ±0.001 | +0.042 ±0.003 |
| 2 | P594 | -2380046.428 | -4593510.547 | 3719463.252 | -0.122 ±0.001 | +0.069 ±0.001 | +0.002 ±0.004 |
| 3 | CCCC | -2412476.008 | -4600711.915 | 3689538.424 | +0.219 ±0.001 | -0.040 ±0.001 | -0.002 ±0.003 |
| 4 | COSO | -2411148.428 | -4571430.096 | 3727461.443 | -0.031 ±0.001 | -0.058 ±0.002 | +0.005 ±0.005 |
| 5 | P580 | -2372609.822 | -4618139.915 | 3695056.934 | -0.018 ±0.001 | +0.189 ±0.001 | -0.001 ±0.003 |
| 6 | BEPK | -2435855.682 | -4566920.654 | 3718714.780 | +0.017 ±0.001 | -0.089 ±0.001 | -0.004 ±0.004 |
| 7 | P464 | -2373746.576 | -4577465.272 | 3742992.407 | -0.088 ±0.001 | -0.020 ±0.001 | +0.044 ±0.004 |
| 8 | P616 | -2434637.188 | -4599523.187 | 3676971.854 | +0.032 ±0.001 | -0.002 ±0.001 | +0.018 ±0.003 |
| 9 | P463 | -2358354.973 | -4595829.858 | 3730988.424 | -0.018 ±0.001 | +0.023 ±0.001 | -0.020 ±0.003 |
| 10 | RAMT | -2420453.848 | -4613541.753 | 3669398.901 | +0.090 ±0.001 | +0.014 ±0.001 | -0.004 ±0.003 |
| 11 | P593 | -2380402.478 | -4630755.979 | 3673829.448 | +0.021 ±0.001 | +0.023 ±0.001 | -0.013 ±0.002 |
| 12 | P570 | -2456509.109 | -4569864.797 | 3698741.097 | +0.007 ±0.001 | -0.040 ±0.001 | -0.004 ±0.003 |
| 13 | P597 | -2345289.073 | -4625138.101 | 3702862.908 | -0.000 ±0.001 | +0.055 ±0.001 | +0.002 ±0.003 |
| 14 | P569 | -2454606.504 | -4592482.980 | 3672875.728 | +0.015 ±0.001 | -0.009 ±0.001 | +0.003 ±0.003 |
| 15 | P592 | -2392604.453 | -4634944.761 | 3660120.000 | +0.040 ±0.001 | +0.002 ±0.001 | -0.010 ±0.003 |
| 16 | P573 | -2444058.864 | -4546615.973 | 3737981.868 | +0.008 ±0.001 | -0.027 ±0.001 | +0.003 ±0.003 |
| 17 | GOL2 | -2353614.546 | -4641385.241 | 3676976.383 | -0.005 ±0.001 | +0.028 ±0.001 | -0.003 ±0.004 |
| 18 | P590 | -2401018.649 | -4639017.208 | 3648862.122 | +0.039 ±0.001 | -0.000 ±0.001 | +0.015 ±0.004 |
| 19 | CPBN | -2419255.381 | -4632919.797 | 3644863.406 | +0.036 ±0.001 | -0.019 ±0.001 | -0.025 ±0.003 |
| 20 | P591 | -2452572.208 | -4609419.087 | 3652114.218 | +0.023 ±0.001 | -0.004 ±0.001 | -0.052 ±0.003 |
| 21 | P466 | -2393286.999 | -4541296.825 | 3777361.154 | -0.020 ±0.001 | -0.001 ±0.001 | +0.005 ±0.003 |
| 22 | P465 | -2422489.483 | -4530744.609 | 3771699.953 | -0.006 ±0.001 | -0.003 ±0.001 | +0.013 ±0.003 |
| 23 | LNMT | -2367549.736 | -4658701.420 | 3646833.090 | +0.001 ±0.001 | +0.005 ±0.001 | +0.012 ±0.003 |
| 24 | P615 | -2349747.713 | -4659201.481 | 3657011.880 | +0.001 ±0.001 | +0.005 ±0.001 | -0.001 ±0.003 |
| 25 | P617 | -2330817.047 | -4660292.842 | 3667462.732 | -0.002 ±0.001 | +0.011 ±0.001 | +0.003 ±0.003 |

Table 2 shows that the four farthest GNSS stations with the neglectable slip values are P465, LNMT, P615, and P617. However, the effects of the earthquake on these stations are still observed in Fig. 4. Since these stations are about 100km from the epicenter, the effect of the earthquake for farther stations can be ignored. The closest station P595 was shifted nearly 0.6m in the south-east direction. Another nearby GNSS station (CCCC) was shifted approximately 0.2 m but in the opposite direction.

Figure 4 shows the north, east and up series of 17 remaining GNSS stations. The timing of the earthquake-induced movement is well documented on the charts of the stations. It may vary with the distance to the epicenter but cannot be observed if it is less than 15 seconds.

We present displacement vectors of the affected stations in Fig. 5, and clearly see that the displacements of GNSS stations decrease with distance away from the epicenter. The displacements of GNSS stations follow to three main directions: north-south direction for stations concentrated in the south of the epicenter, south-east direction for stations in the east and south-west direction for stations in the north-west.

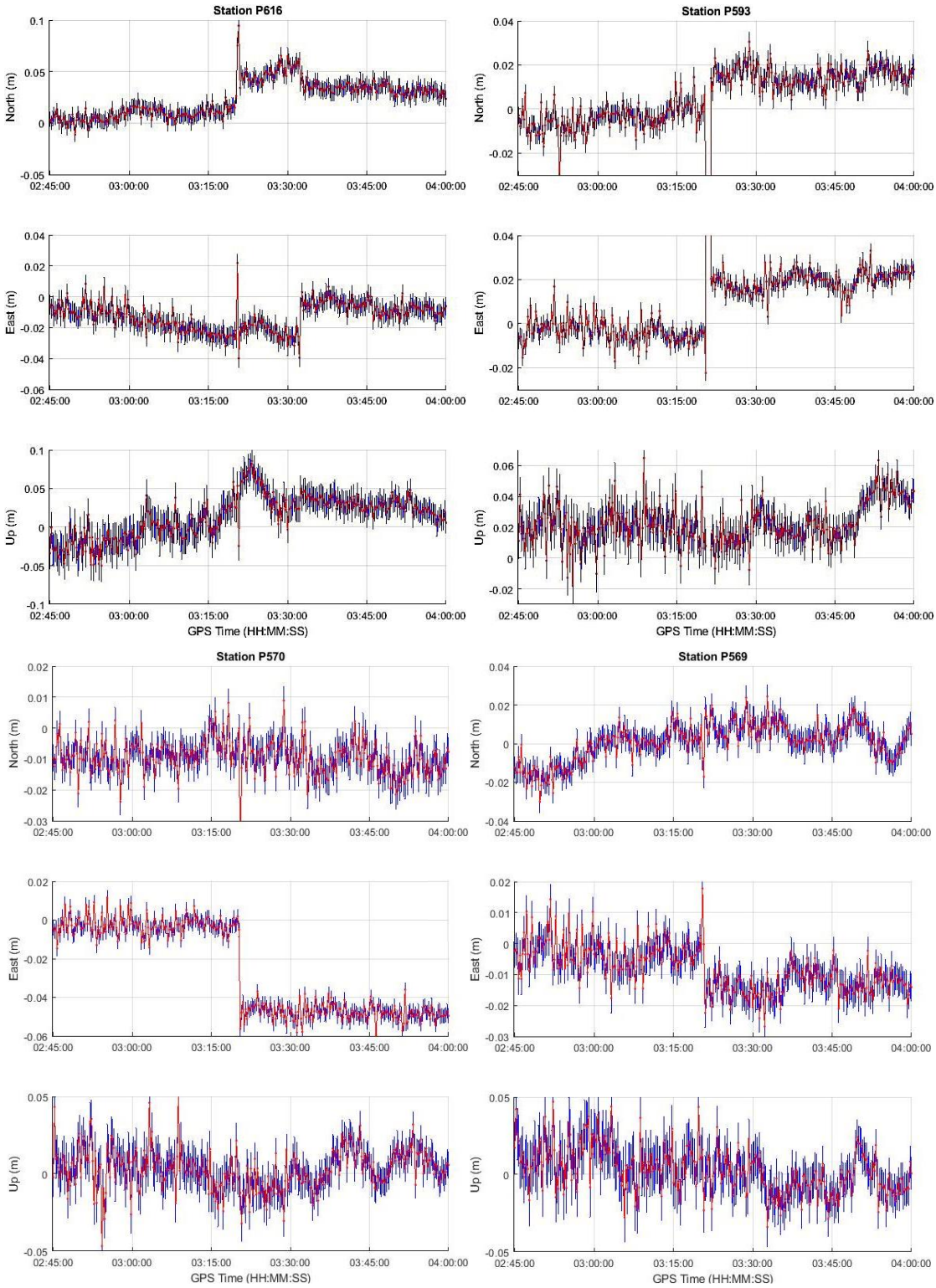


*Figure 4*. The coordinate series over time of the 17 remaining GNSS stations

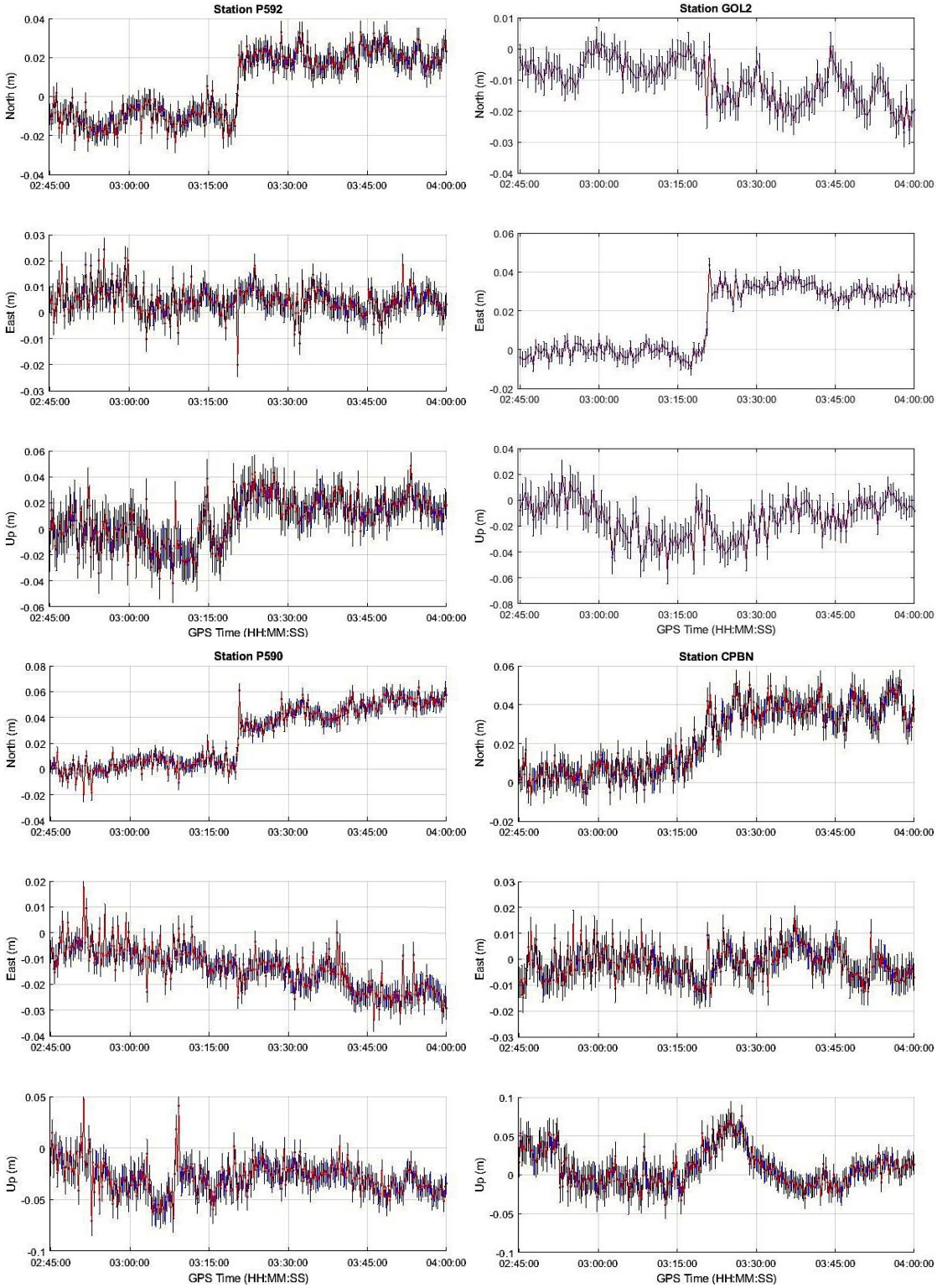


*Figure 4 (continuous)*

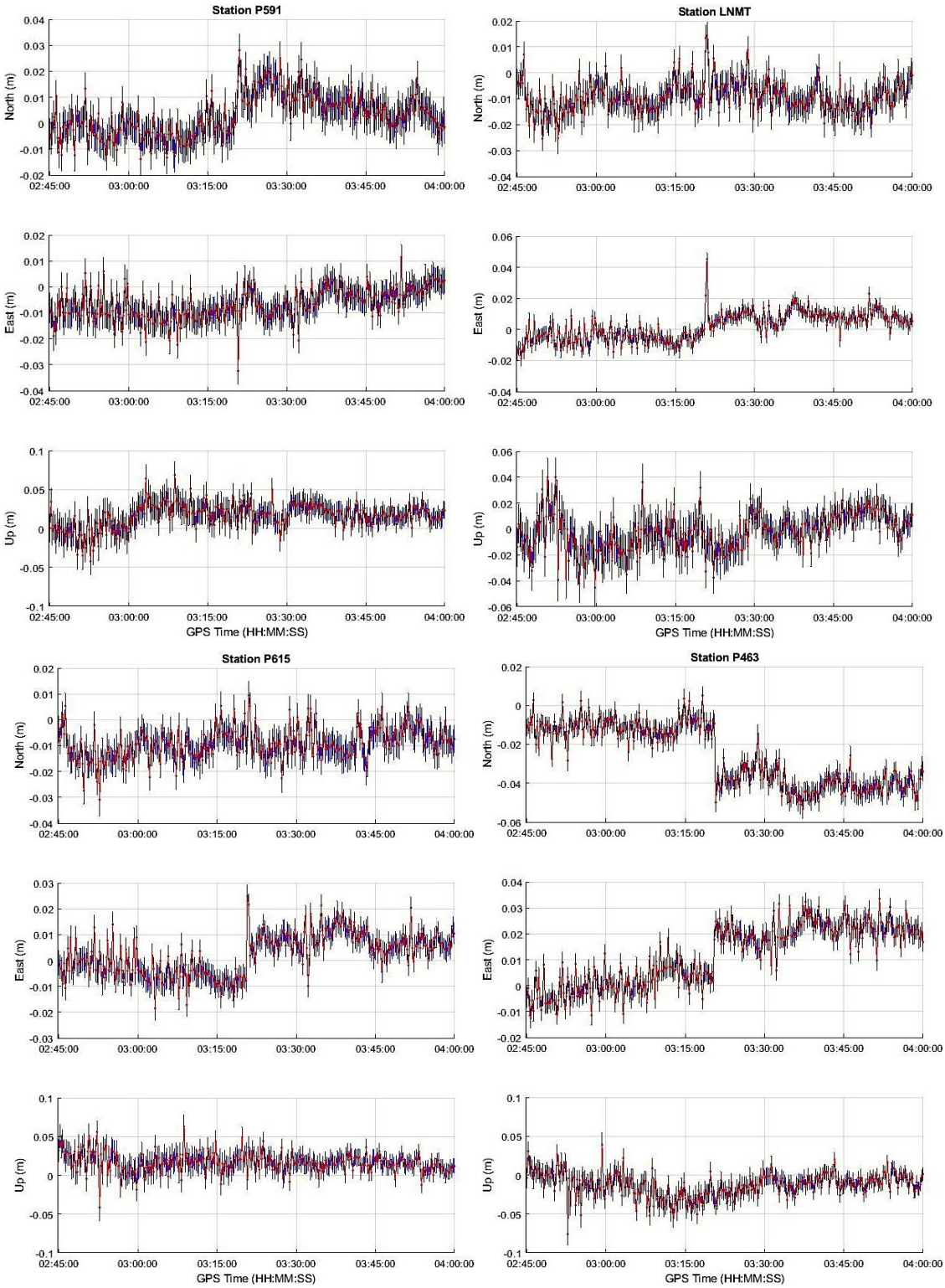


*Figure 4 (continuous)*

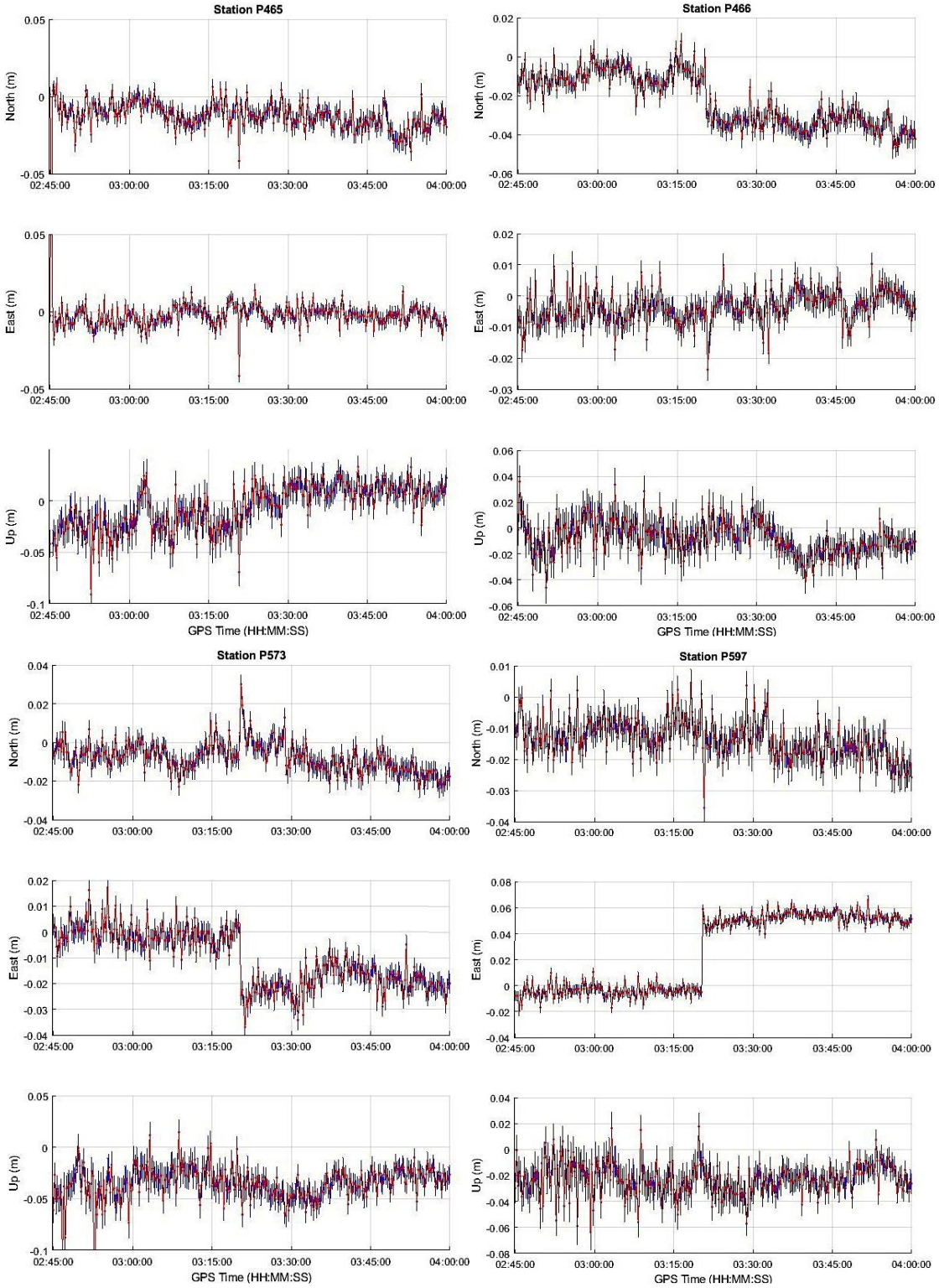


*Figure 4 (continuous)*

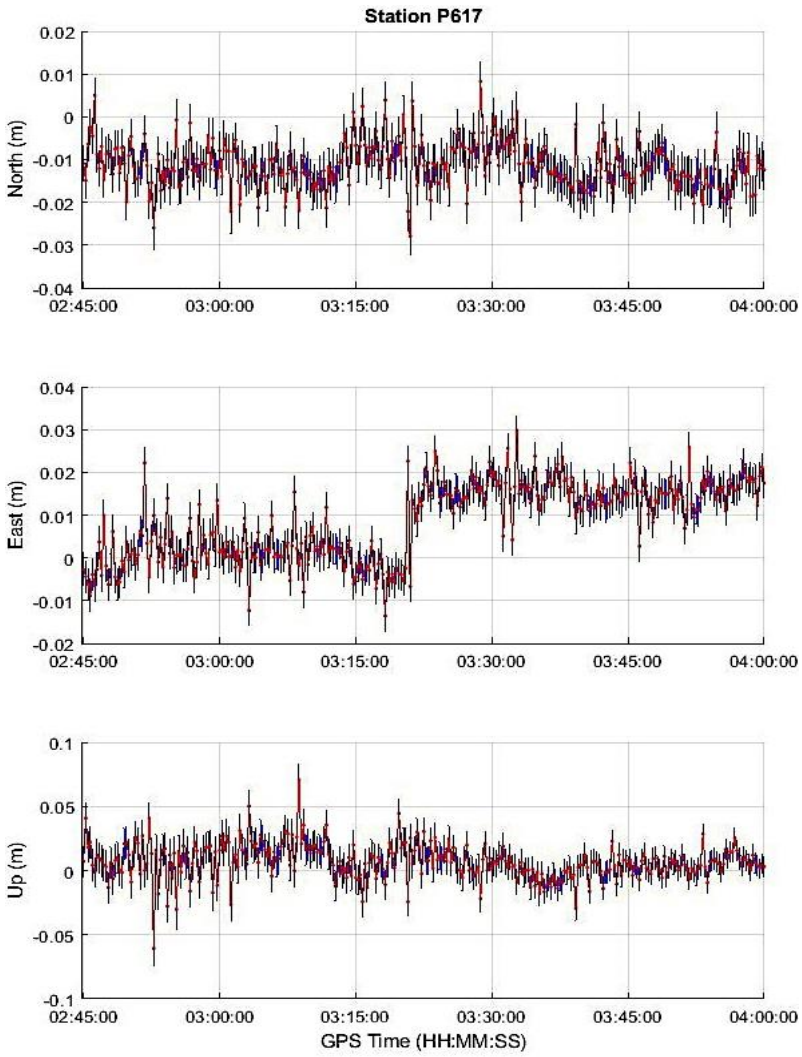


*Figure 4 (continuous)*

## 5. Discussions

Based on the data recorded by NOTA GNSS stations streaming high-rate (1-sps/1 Hz) data in real time, Phillips and Bartel (2019) calculated the displacement traces within second of the earthquake (see Fig. 6). Coseismic offsets from this event have been estimated by the GAGE GNSS Analysis Centers. Preliminary "rapid" offsets of some GNSS stations have been tabulated in Table 3.

Compared to Table 3 with our results in Table 2, we can see the deviation of the most stations at cm level, except stations P595 at ~1 dm in the East component. The deviation between the two results is due to some follow reasons:

- Using the different rates of the GNSS data: interval of 1 second vs. 15 seconds.
- They used the station coordinates processed by RTK method with the rapid orbit, while we used the PPP-AR method with the final CNES products.
- To calculate the displacement, they use the station coordinates within seconds after the earthquake, while we estimated the station coordinates for the long segments.

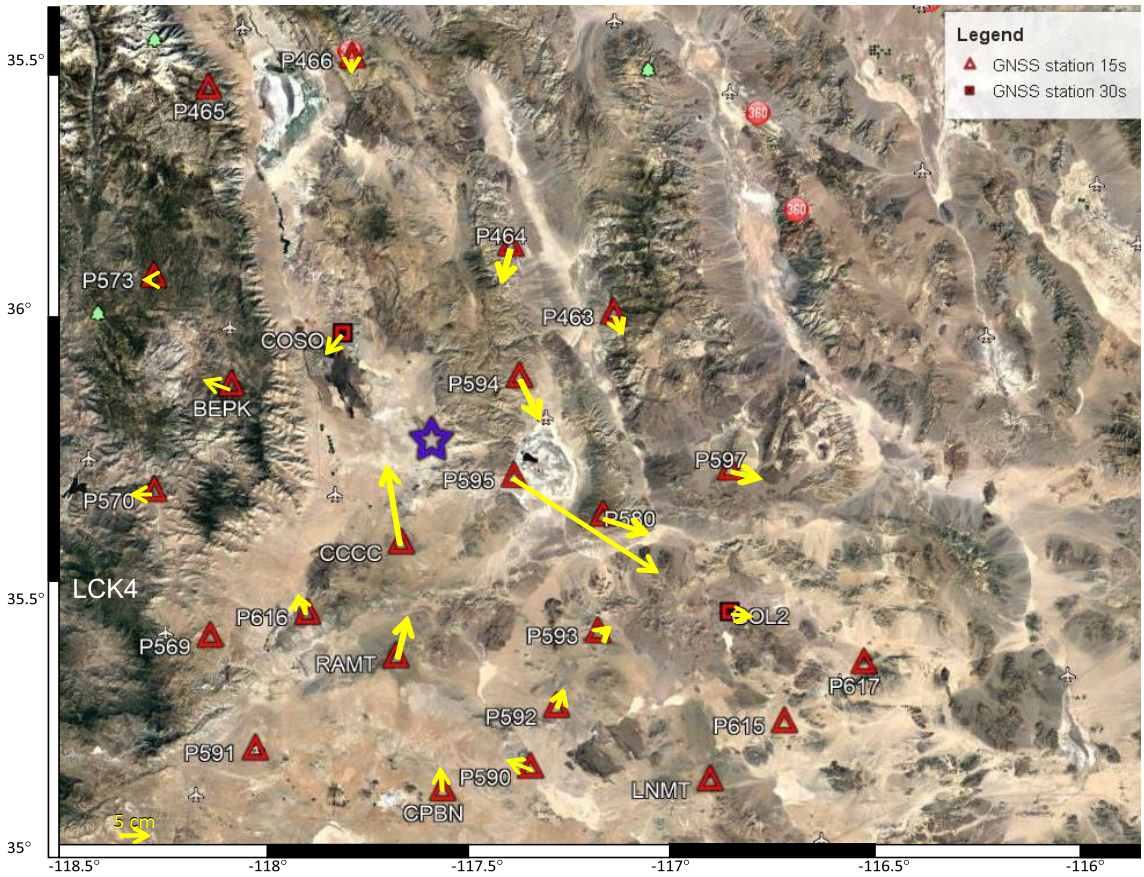


*Figure 5*. Co-seismic ground displacements determined by PPP method from 25 permanent GNSS stations in the 6 July 2019 Ridgecrest earthquake

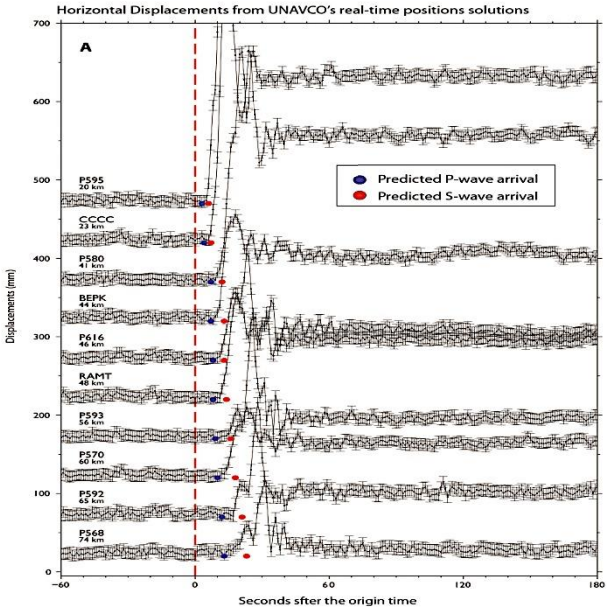


*Figure 6*. The coordinate series over time of the 10 GNSS stations from (Phillips and Bartel, 2019)

*Table 3*. Preliminary "rapid" offsets of some GNSS stations by the GAGE GNSS Analysis Centers

| No. | GNSS Station | Displacements (m) | | | Deviations (m) | | |
|---|---|---|---|---|---|---|---|
| | | North | East | Up | North | East | Up |
| 1 | P595 | -0.250 | +0.625 | +0.058 | +0.001 | +0.109 | +0.016 |
| 2 | P594 | -0.151 | +0.069 | +0.012 | -0.029 | +0.000 | +0.010 |
| 3 | CCCC | +0.216 | -0.082 | +0.013 | -0.003 | -0.042 | +0.011 |
| 4 | COSO | -0.041 | -0.064 | +0.006 | -0.010 | -0.006 | +0.011 |
| 5 | P580 | -0.026 | +0.221 | -0.004 | -0.008 | +0.032 | -0.005 |
| 6 | BEPK | +0.015 | -0.101 | -0.007 | -0.002 | -0.012 | -0.003 |
| 7 | P464 | -0.103 | -0.021 | +0.014 | -0.015 | -0.001 | -0.030 |
| 8 | P616 | +0.041 | -0.010 | +0.010 | +0.009 | -0.012 | -0.008 |
| 9 | P463 | -0.028 | +0.021 | +0.006 | -0.010 | -0.002 | +0.025 |
| 10 | RAMT | +0.100 | +0.013 | +0.009 | +0.010 | -0.001 | +0.013 |

The large deviations in the East component of station P595 and CCCC, in our opinion, are due to the large variations of the coordinates of these stations in the seconds right after the earthquake occurs. It leads to inaccurate calculation of the station displacements. Fortunately, such large values are not observed in the 15s GNSS data (Fig. 7).

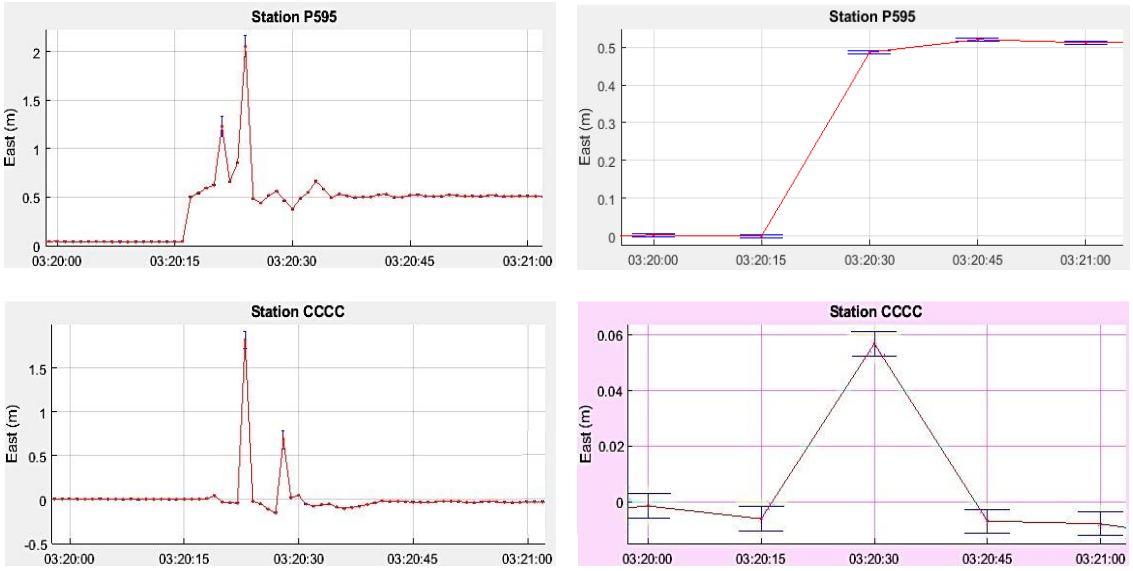


*Figure 7*. Coordinate series of station P595 (top) and CCCC (bottom) in the East component from processing 1s (left) and 15s GNSS data (right)

On the other hand, from Figure 4, we can see obviously that the shifting time of the stations has a gradual increase with their distance to the epicenter. However, the difference between the nearest station (P595) and the station 74km (P568) is still less than 15 seconds. This is why we have not observed this on our results.

## 6. Conclusions

To monitor the effect of the earthquake with a magnitude of 7.1 on 7 July 2019 in eastern California, we collected and processed GNSS data at 25 stations around the epicenter by using the GNSS PPP method with AR. The GNSS station displacements are calculated precisely with an accuracy of 1cm in the

horizontal and the vertical components. These displacements show that the affected area stretches about 100 km around the epicenter. The closest GNSS station is shifted in the south-east direction with the maximum value of 0.6m in the horizontal component.

## Acknowlegments

Phan T.T. thank the senior research assistant Program of Vietnam Academy of Science and Technology.

## References

Akram Afifi, Ahmed El-Rabbany, 2016. Improved Between-Satellite Single-Difference Precise Point Positioning Model Using Triple GNSS Constellations: GPS, Galileo, and Beidou, Positioning, 7, 63–74.

Garrett Seepersad and Sunil Bisnath, 2016. Examining the interoperability of precise point positioning products, GPS World, 27(3), 50–56.

Geospatial Information Authority of Japan, https://www.gsi.go.jp/ENGLISH/index.html.

Han Yue, Thorne Lay, Susan Y. Schwartz, Luis Rivera, Marino Protti Timothy H. Dixon, Susan Owen, and Andrew V. Newman, 2013. The 5 September 2012 Nicoya, Costa Rica Mw 7.6 earthquake rupture process from joint inversion of high-rate GPS, strong-motion, and teleseismic P wave data and its relationship to adjacent plate boundary interface properties. Journal of Geophysical Research: Solid Earth, 118, 5453–5466. Doi:10.1002/jgrb.50379.

Ji C., Larson K.M., Tan Y., Hudnut K.W., Choi K., 2004. Slip history of the 2003 San Simeon earthquake constrained by combining 1-Hz GPS, strong motion, and teleseismic data. Geophysical Research Letters, 31(17), L17608, 10.1029/ 2004GL020448c.

Jianghui Geng, Chuang Shi, Maorong Ge, Alan H. Dodson, Yidong Lou, Qile Zhao, Jingnan Liu, 2012. Improving the estimation of fractional-cycle biases for ambiguity resolution in precise point positioning. Journal of Geodesy, 86, 579–589.

Junbo Shi, 2012. Precise Point Positioning Integer Ambiguity Resolution with Decoupled Clocks, PhD Thesis at the University of Calgary, Canada.

King M., Edwards S., Peter Clarke, 2002. Precise Point Positioning: Breaking the Monopoly of Relative GPS Processing. Engineering Surveying Showcase 10/2002, 33–34.

Kouba J., 2009. A Guide to using International GNSS Service (IGS) products, Natural Resources Canada, http://igscb.jpl.nasa.gov/components/usage.html.

Laurichesse D., 2012. Phase Biases Estimation for Undifferenced Ambiguity Resolution, PPP-RTK & Open Standards Symposium, March 12-13, Frankfurt.

Mahmoud Abd Rabbou, Ahmed El-Rabbany, 2015. PPP Accuracy Enhancement Using GPS/GLONASS Observations in Kinematic Mode, Positioning, 6, 1–6.

Nguyen Ngoc Lau, 2017. Accuracy of PPP with ambiguity resolution in the ITRF2014, The 15th Conference of Science and Technology organized by the Ho Chi Minh City University of Technology, Ho Chi Minh City.

Nguyen Ngoc Lau, Duong Minh Au, Nguyen Van Tuan, Dang Van Cong Bang, 2012. Precise point positioning using GPS and GLONASS measurements, Report of ministry-level of project B2012-20-33.

Phillips D., Bartel B., 2019. Data Event Response to the July 4, 2019 M 6.4 and July 6, 2019 M 7.1 Earthquakes Near Ridgecrest, California, UNAVCO https://www.unavco.org/highlights/2019/ridgecrest.html.

Shuyang Cheng, Jinling Wang, 2016. Ambiguity Resolution (PPP-AR) For Precise Point Positioning Based on Combined GPS Observations, International Global Navigation Satellite Systems Association IGNSS Conference 2016, Colombo Theatres, Kensington Campus, UNSW Australia 6–8, December 2016.

SOPAC, 2019, http://sopac-csrc.ucsd.edu/.

Stein R.S., Hobbs T., Rollins Ch., Ely G., Sevilgen V., Toda S., 2019a. Magnitude 7.1 Earthquake rips northwest from the M6.4 just 34 hours later.

Temblor, http://52.24.98.51/earthquake-insights/magnitude-7-1-earthquake-rips-northwest-from-the-m6-4-just-34-hours-later-9041/.

Stein R.S., Rollins Ch., Sevilgen V., Hobbs T., 2019b. M 7.1 SoCal earthquake triggers aftershocks up to 100 mi away: What's next?, Temblor, http://doi.org/10.32858/temblor.038.

USGS, 2019, https://earthquake.usgs.gov/earthquakes/eventpage/ci38457511/executive.

Zumberge J.F, Heflin M.B., Jefferson D.C., Wattkins M.M., Webb F.H., 1997. Precise point positioning for the efficient and robust analysis of GPS data from large networks, Journal of Geophysical Research, 102(B3), 5005–5017.